An Adaptive Sampling Technique for Passivity Characterization and Enforcement of Large Interconnect Macromodels

Stefano Grivet-Talocia, *Senior Member, IEEE*

***Abstract*—This paper deals with the characterization and enforcement of passivity for linear lumped interconnect macromodels. An adaptive accuracy-controlled frequency sampling process is employed to identify a set of frequency bands where the macromodel is locally passive. These results are employed as a preliminary step, enabling the fast computation of imaginary eigenvalues of the Hamiltonian matrix associated to the macromodel. Then, iterative perturbation is employed to remove these eigenvalues from the imaginary axis and to achieve global passivity. The resulting scheme is highly optimized for macromodels having large dynamic order and with a sparse structure. Significant speedup factors up to two orders of magnitude are achieved with respect to a standard implementation of the same passivity compensation scheme based on a full eigensolver.**

***Index Terms*—Adaptive sampling, Arnoldi algorithm, complex frequency hopping, eigenvalues, Hamiltonian matrices, linear macromodeling, passivity, perturbation theory, scattering, singular values, sparse matrices.**

I. Introduction

MACROMODELING is nowadays a common practice for the assessment of signal integrity (SI) issues in early stages of the design of complex high-speed electronic systems. A common approach to system-level SI analysis is to partition a complex interconnected system into several different and well-defined structures, like e.g., transmission line segments, via fields, connectors, discontinuities, etc. Each structure is separately analyzed via full-wave solvers in time or frequency domain or via direct measurements (when possible), in order to derive its electromagnetic behavior over an extended frequency band. Then the results are processed by suitable fitting/identification algorithms leading to some closed-form representation of the associated transfer matrix in the Laplace domain, rational approximations being the standard choice for lumped models. Finally, the various submodels are cast in a common format (e.g., SPICE or VHDL-AMS) and interconnected for system-level Signal Integrity analyses.

The final simulation step may seem straightforward, but in fact serious difficulties may be encountered if any of the different macromodels is not passive. In fact, nonpassive components may lead to unstable transient simulations due to their ability to generate more energy than they are fed with. Some examples illustrating this loss of stability are available in [24] and [26]. This is indeed a serious drawback that in some cases makes the macromodels practically useless. Consequently, there is a strong motivation underlying several research efforts by both academia and industry towards efficient schemes for the enforcement of the macromodel passivity. Several schemes have been proposed so far. We can cite approaches based on *a priori* assumptions on the macromodel representation [15], on linear or quadratic programming based on a discrete set of frequencies [16], [23], on convex optimization with passivity constraints [17]–[19], and on Hamiltonian matrices [21], [22], [24]–[26]. When the macromodel size is limited, such schemes run with moderate requirements of computational resources. However, their applicability to large-sized macromodels is quite limited due to the excessive computational cost involved in the passivity enforcement.

Here, we concentrate on the class of methods based on the iterative perturbation of Hamiltonian eigenvalues. In fact, there is still significant potential for improving their efficiency when the number of internal states, or equivalently, the number of poles of the macromodel is large. In this work, we show that an accuracy-controlled adaptive frequency sampling process, combined with a customized scheme for the determination of few Hamiltonian eigenvalues restricted to small frequency intervals, may result in very significant speedup factors with respect to more standard implementations. In some cases, speedup factors up to two orders of magnitude have been observed without affecting the quality of the results.

More detailed preliminaries and motivations for the developments in this work are provided in Section II. The proposed adaptive sampling scheme is presented in Section III. The algorithms for the determination of the imaginary eigenvalues of the Hamiltonian matrix and for the passivity compensation are summarized in Section IV. Finally, numerical examples will follow in Section V.

II. Preliminaries and Motivations

We consider linear macromodels in state-space form

$$\begin{cases} \dot{\boldsymbol{x}}(t) = \boldsymbol{A}\boldsymbol{x}(t) + \boldsymbol{B}\boldsymbol{u}(t) \\ \boldsymbol{y}(t) = \boldsymbol{C}\boldsymbol{x}(t) + \boldsymbol{D}\boldsymbol{u}(t) \end{cases} \tag{1}$$

having N poles (size of $\boldsymbol{A}$), with corresponding $P \times P$ transfer matrix

$$\boldsymbol{H}(s) = \boldsymbol{D} + \boldsymbol{C}(s\boldsymbol{I} - \boldsymbol{A})^{-1}\boldsymbol{B}. \tag{2}$$

Manuscript received February 10, 2006; revised September 20, 2006. This work is supported by the Italian Ministry of University (MIUR) under a Program for the Development of Research of National Interest (PRIN Grant 2004093025).

The author is with the Department of Electronics, Politecnico di Torino, Torino 10129, Italy (e-mail: stefano.grivet@polito.it).

Digital Object Identifier 10.1109/TADVP.2007.895990

Only the scattering representation will be considered for (1) and (2), but all the results in this work will be applicable with obvious modifications to other representations, e.g., impedance or admittance [25]. The macromodel in the state-space form (1) can be obtained by applying some fitting algorithm, such as the well-known Vector Fitting [8], to estimate poles and residues from frequency-domain tabulated scattering parameters of the structure under investigation. We assume that all poles, or equivalently the eigenvalues of $\boldsymbol{A}$, are strictly stable, so that the transfer (scattering) matrix $\boldsymbol{H}(s)$ is nonsingular for $\Re\{s\} \geq 0$. Since all state matrices are assumed real, the passivity of $\boldsymbol{H}(s)$ can be checked only on the purely imaginary axis $s = j\omega$ by insuring that all singular values of $\boldsymbol{H}(j\omega)$ must be uniformly bounded by one at any frequency

$$\sigma_i \leq 1, \quad \forall \sigma_i \in \sigma\left(\boldsymbol{H}(j\omega)\right), \quad \forall \omega. \tag{3}$$

This condition is equivalent to

$$\left(\boldsymbol{I} - \boldsymbol{H}^H(j\omega)\boldsymbol{H}(j\omega)\right) \geq 0, \quad \forall \omega \tag{4}$$

where ^{H} denotes complex conjugate transpose. In the following, we will also assume asymptotic passivity (i.e., the singular values of $\boldsymbol{D}$ are strictly less than one), together with controllability and observability of the state-space realization (1). These two conditions are easily enforced as described in [26]. Finally, we will only work with macromodels in sparse form as discussed in [26] and [35], characterized by sparse state-space matrices. The basic condition underlying all developments requires that $(j\omega\boldsymbol{I} - \boldsymbol{A})$ can be inverted at a small computational cost. Therefore, we will assume $\boldsymbol{A}$ to be block-diagonal, with blocks of size 1 for the synthesis of real poles and of size 2 for complex pole pairs. Note that this choice is always possible in the construction of the state-space realization and leads to a $O(N)$ computational cost for the evaluation of the transfer matrix at a given frequency.

The well-known theory of Hamiltonian matrices [20], [25] identifies the frequencies ω_k at which one of the singular values σ_i reaches the threshold $\gamma = 1$ with the purely imaginary eigenvalues $\mu_k = j\omega_k$ of the Hamiltonian matrix

$$\mathcal{M} = \begin{pmatrix} \boldsymbol{A} - \boldsymbol{B}\boldsymbol{R}^{-1}\boldsymbol{D}^T\boldsymbol{C} & -\boldsymbol{B}\boldsymbol{R}^{-1}\boldsymbol{B}^T \\ \boldsymbol{C}^T\boldsymbol{S}^{-1}\boldsymbol{C} & -\boldsymbol{A}^T + \boldsymbol{C}^T\boldsymbol{D}\boldsymbol{R}^{-1}\boldsymbol{B}^T \end{pmatrix} \tag{5}$$

where $\boldsymbol{R} = (\boldsymbol{D}^T\boldsymbol{D} - \boldsymbol{I})$ and $\boldsymbol{S} = (\boldsymbol{D}\boldsymbol{D}^T - \boldsymbol{I})$.

If some imaginary eigenvalues are found, the macromodel is not passive and compensation must be performed. The iterative perturbation scheme of [21] and [25] can be used to displace these eigenvalues from the imaginary axis and to achieve passivity. No details about the main algorithm will be provided here, since they are available in the open literature. We recall that the main numerical tools required by this scheme are eigenvalue determinations and least squares solutions of small linear systems. In other words, the compensation is performed via algebraic operations that do not need frequency sampling for checking and/or enforcing (3). On the other hand, the need of an eigensolution of the Hamiltonian matrix becomes a weak point when the dynamic order N is large, since the associated cost scales as $O(N^3)$. As a consequence, when a standard full eigensolver is employed, the standard Hamiltonian-based scheme of [21] and [25] can only be applied to moderate-size macromodels with a reasonable computational cost. We remark that the same cubic scaling law applies to the computational cost per iteration of state-of-the art convex optimization approaches [17]. Here, we are trying to reduce this cost.

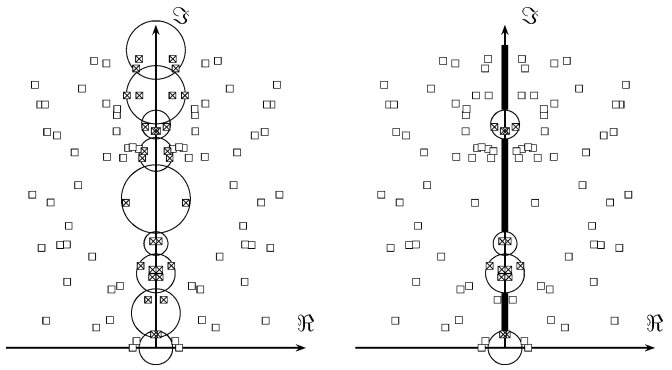

Fig. 1. Use of multiple shifts along the imaginary axis for the determination of few eigenvalues of the Hamiltonian matrix close to the imaginary axis (crosses), neglecting the other part of the eigenspectrum (squares). Circles indicate the convergence regions for the restarted Arnoldi process at each shift. The entire bandwidth is processed in left panel, thus requiring a possibly large number of shifts. Right panel shows that a significant reduction in the number of shifts may be achieved by skipping some carefully selected frequency intervals (thick lines).

Some progress in speeding up the algorithm has been documented in [26] and [35]. In these works, a dedicated eigensolver for the selective determination of the imaginary eigenvalues of Hamiltonian matrices admitting sparse decompositions was presented. This eigensolver is based on a multishift restarted Arnoldi process [30], [31], [39], similar to the complex frequency hopping (CFH) scheme [32]. A bisection process is performed on the full bandwidth encompassing all imaginary eigenvalues (if present), and multiple shifts are placed along the imaginary axis. A dedicated Arnoldi process aimed at the determination of few closest eigenvalues to each shift is run, and the results are collected to gather the full set of imaginary eigenvalues. All details are reported in [26] and [35], and a schematic illustration is provided in the left panel of Fig. 1. The advantage of this scheme in terms of required operations is significant, since the computational cost scales with the number of states only linearly, as $O(cN)$. Unfortunately, the constant c may be very large, since it is roughly proportional to the number of shifts and to the squared size of the Krylov subspace being used at each shift, the main bottleneck being the unavoidable orthogonalization of the Krylov vectors. In particular cases characterized by a Hamiltonian eigenspectrum clustered around the imaginary axis, the number of shifts grows very large and the speedup factor with respect to a standard full eigensolver results quite moderate. These difficulties are documented in [26].

The above considerations lead to the conclusion that a reduction of the number of shifts could significantly improve the efficiency of the entire compensation scheme. This is indeed the purpose of this work. We show that an adaptive sampling process can be applied to identify the strictly passive frequency bands, where no imaginary eigenvalues can be located, by checking (3) or (4) directly at carefully selected frequencies. Although it is widely recognized that this procedure may be

cumbersome and computationally expensive, this is not the case when a fast inversion of $(j\omega\boldsymbol{I}-\boldsymbol{A})$ is possible and when $N \gg P$. It is obvious that this identification is however only approximate, since only a finite number of frequency samples are tested. Indeed, we will use this frequency sweep test only as a preliminary step, aimed at the exclusion of a set of certainly passive frequency bands from the more accurate but expensive check based on the imaginary Hamiltonian eigenvalues. The multishift eigensolver, applied to these reduced-size frequency bands, will only need a reduced number of shifts with respect to its full-bandwidth application, as depicted in the right panel of Fig. 1. Consequently, the computational cost will be significantly reduced. Preliminary results of the proposed adaptive sampling techniques were available in [27]. The following high-level list illustrates the various steps of the proposed algorithm, pointing out the section where the details are developed.

1) Perform an accurate frequency sampling of $\boldsymbol{H}(j\omega)$ (Section III):
   a) estimate the upper frequency (Section III-A);
   b) perform an initial coarse sampling (Section III-B);
   c) iteratively refine the frequency samples until sufficiently accurate (Section III-C).
2) Extract the frequency bands where $\boldsymbol{H}(j\omega)$ is certainly passive (Section III-D).
3) Apply a multishift process to each of the remainig frequency bands and collect all imaginary Hamiltonian eigenvalues (Section IV and [26]).

III. Adaptive Sampling

This section presents an adaptive frequency sampling technique aimed at the detection of frequency bands where local passivity is guaranteed. More precisely, the expected result is a collection of frequency intervals

$$\Omega^{\text{passive}} = \bigcup_{q=1}^{Q} \Omega_q, \quad \Omega_q = (\omega_{q,0}, \omega_{q,1}) \tag{6}$$

such that

$$\sigma_i < 1, \quad \forall \sigma_i \in \sigma\left(\boldsymbol{H}(j\omega)\right), \quad \forall \omega \in \Omega^{\text{passive}}. \tag{7}$$

It will be convenient to work with the squared singular values $\lambda_i = \sigma_i^2$, which are subject to the same unitary boundedness condition (7) for passivity. The λ_i are the eigenvalues of the Hermitian matrix

$$\boldsymbol{\Theta}(j\omega) = \boldsymbol{H}^H(j\omega)\boldsymbol{H}(j\omega) \tag{8}$$

and are therefore strictly real and positive. We will collect the associated eigenvectors, denoted as $\boldsymbol{v}_i$, in the modal matrix $\boldsymbol{V}$. Due to the fundamental properties of Hermitian matrices we have

$$\begin{aligned} \boldsymbol{V}^H(j\omega)\boldsymbol{\Theta}(j\omega)\boldsymbol{V}(j\omega) &= \operatorname{diag}\left\{\lambda_i(j\omega)\right\}, \\ \boldsymbol{V}^H(j\omega)\boldsymbol{V}(j\omega) &= \boldsymbol{I} \quad \forall\omega. \end{aligned} \tag{9}$$

We remark that even in case of λ_i with multiplicity larger than one, there always exists a modal matrix $\boldsymbol{V}$ satisfying (10), since $\boldsymbol{\Theta}$ cannot be defective [33].

The generation of the frequency samples follows a sequence of steps that are itemized below.

1) Estimate the frequency $\omega_{\max}$ providing an upper bound for all imaginary eigenvalues $j\omega_k$ of the Hamiltonian matrix. The existence of this upper frequency is guaranteed by the asymptotic passivity of the macromodel, here assumed *a priori*.
2) Generate an initial set of frequency samples based on the distribution of the macromodel poles.
3) Check and iteratively refine the set of frequency samples so that tracking of individual eigenvalues λ_i and associated eigenvectors $\boldsymbol{v}_i$ is achieved throughout $[0, \omega_{\max}]$.

These steps are detailed in Sections III-A–III-C. Finally, in Section III-D, we illustrate the procedure for the determination of Ω^{passive}.

A. Upper Frequency

The upper frequency $\omega_{\max}$ is quite easy to estimate. In fact, it is sufficient to have an estimate of the eigenvalue of maximum magnitude of the Hamiltonian matrix $\mathcal{M}$

$$|\mu_{\max}| = \arg\max_k |\mu_k| \tag{10}$$

since by definition

$$\omega_{\max} \leq |\mu_{\max}|. \tag{11}$$

The evaluation of the maximum magnitude eigenvalue is a standard problem in numerical analysis, since the sequence

$$\{\boldsymbol{x}, \mathcal{M}\boldsymbol{x}, \mathcal{M}^2\boldsymbol{x}, \ldots\} \tag{12}$$

with proper normalization converges to the associated eigenvector. This is the basis of all Krylov-subspace projection methods for selective eigenvalue determination. The reader is referred to any numerical analysis text for details (see, e.g., [31] and [38]). We note here that the construction of the above sequence only requires the application of the Hamiltonian matrix to a given starting vector. This operation requires at most $4N(P+1)+4P^2$ operations, using the formulation of [26]. Therefore, the estimation of $\omega_{\max}$ can be performed at a cost that is negligible with respect to the overall cost of the passivity compensation process. Once $\omega_{\max}$ is known, we can safely assume that all imaginary eigenvalues (if any) $\mu_k = j\omega_k$ of the Hamiltonian matrix are such that $\omega_k \in [0, \omega_{\max}]$. Also, this implies that the rightmost strictly passive frequency band in (6) extends to infinity and is expressed as $\Omega_Q = (\omega_{\max}, \infty)$.

B. Initial Sampling

A starting set of frequency samples providing a rough representation of the frequency-dependent eigenvalues $\lambda_i(j\omega)$ can be determined by the distribution of the macromodel poles $p_n = \alpha_n + j\beta_n$. These poles are known since, due to the assumptions

on the state-space realization, their real parts are the diagonal entries of $\boldsymbol{A}$ and their imaginary parts are placed in the first order diagonals. Each macromodel pole contributes to the frequency variation of the transfer matrix (hence of the eigenvalues λ_i) mostly in a bandwidth centered at β_n with size approximately $|\alpha_n|$. This is evident from the partial fraction expansion of (2)

$$\boldsymbol{H}(s) = \boldsymbol{D} + \sum_n \frac{\boldsymbol{R}_n}{s - p_n} \tag{13}$$

showing that the frequency variations of $\boldsymbol{H}(j\omega)$ are due to the superposition of the various partial fraction terms, each being associated to a single pole. The highly resonant poles induce local variations and require fine sampling around the resonant frequency. Conversely, highly damped poles induce smooth variations, requiring a coarse and spread grid.

There are several choices for the generation of frequency samples that well represent both magnitude and phase variations associated to each pole. Here, we consider a total number of $2R+1$ frequency samples for each pole (only the poles with nonnegative imaginary part are considered), expressed as

$$\omega_{n,r} = \beta_n + \alpha_n \tan \frac{r\pi}{2(R+1)} \quad r = -R, \ldots, R. \tag{14}$$

These samples provide a uniform sampling of the phase associated to each partial fraction term in (13). A small number of samples per pole is needed. We used $R = 3$ in all numerical tests of this work, which proved to be sufficient.

The samples generated for each pole are accumulated and sorted. Then, only the frequencies enclosed in $[0, \omega_{\max}]$ are retained, including the boundary samples. The resulting number of samples is approximately $(2R+1)N$. However, a last scan is performed to remove those samples that are closer than a prescribed threshold $\Delta\omega$. This step is necessary since the samples coming from different poles may become very close or even coincident. For instance, repeated poles (hence repeated samples) occur when the state-space realization is constructed from a partial fraction representation (13) with residue matrices $\boldsymbol{R}_n$ having rank larger than one [36]. Repeated samples are unnecessary and detrimental for the algorithm to be presented. Various criteria for the determination of the threshold $\Delta\omega$ can be adopted, e.g., any combination of the conditions as follows.

- A prescribed portion ϑ of the entire bandwidth, $\Delta\omega = \vartheta\omega_{\max}$.
- As above, with ϑ being parameterized with the number of poles, $\vartheta = (N\rho)^{-1}$, with $\rho \gg 1$.
- An interval parameterized by the smallest real part (in magnitude) among all macromodel poles, $\Delta\omega = \nu \min_n |\alpha_n|$, with $\nu < 1$.

The specific choice is not critical, since even a poorly sampled frequency axis will be subject to the iterative and accuracy-controlled refinement detailed next. It is important, however, that the minimum separation $\Delta\omega$ between the retained samples is not too large, otherwise the benefits of the poles-induced initial sampling may be lost. Of course, there is a trade-off between number of samples (hence CPU time) and accuracy of the initial sampling. In this work, we use the second choice with $\rho = 10$.

C. Iterative Refinement and Tracking

We start here with an initial set of frequency samples $\{\omega_m, m = 0, \ldots, M\}$ with $\omega_0 = 0$ and $\omega_M = \omega_{\max}$, determined by the procedure of Section III-B. These samples provide a rough but representative approximation of the frequency dependence of the transfer matrix (2). In particular, occurrence of sharp peaks and rapid phase variations due to the presence of poorly sampled regions is avoided by construction. The purpose of this section is to present a simple iterative refinement strategy leading to an accuracy-controlled sampled frequency axis. The accuracy metric that is relevant here must be related to the frequency variations of the eigenvalues λ_i, since their values are to be used to detect the strictly passive frequency bands Ω^{passive} in (6). It turns out that a more conservative accuracy measure is provided by the eigenvector matrix $\boldsymbol{V}$, which is more sensitive than the eigenvalues to the perturbations induced by frequency variation. For instance, it is well-known that two eigenvectors may become extremely sensitive to perturbations when their eigenvalues are close, even if each individual eigenvalue is well-behaved [33], since the condition number of an eigenvector depends on the gap between its eigenvalue and the closest other eigenvalue [31]. Therefore, we precompute during the initialization phase

- the matrices $\boldsymbol{H}_m = \boldsymbol{H}(j\omega_m)$ and $\boldsymbol{\Theta}_m = \boldsymbol{\Theta}(j\omega_m)$;
- the eigenvalues $\boldsymbol{\Lambda}_m = \operatorname{diag}\{\lambda_i(j\omega_m)\}$;
- the eigenvectors $\boldsymbol{V}_m = \boldsymbol{V}(j\omega_m)$.

We start with the assumption of simple eigenvalues at each frequency sample

$$\lambda_i(j\omega_m) \neq \lambda_{i'}(j\omega_m), \quad \forall i, i', m. \tag{15}$$

This condition will be relaxed later. Let us choose a pair of adjacent samples ω_m and ω_{m+1} and consider the associated eigenvector matrices $\boldsymbol{V}_m$, $\boldsymbol{V}_{m+1}$. We want to determine if we can use these matrices to track each eigenpair from sample m to sample $m+1$. Indeed, if the sampling is accurate enough, the eigenvalues and the eigenvectors at sample $m+1$ will be small perturbations of those at sample m. A precise mathematical form of this statement must take into account two basic facts in order to be applicable to the general case. First: any eigenvector can only be computed up to an arbitrary phase term, since if $\boldsymbol{v}_i$ is an eigenvector also $\boldsymbol{v}_i e^{j\psi_i}$ is an eigenvector for any $\psi_i \in [0, 2\pi)$. Moreover, most numerical eigendecomposition routines only enforce $||\boldsymbol{v}_i|| = 1$, without any explicit control on the phase ψ_i, which may differ from one frequency sample to another. Therefore, we need a parameterization of the eigenvector matrix which takes into account this arbitrary and unknown phase factors. To this end, we define a diagonal matrix $\boldsymbol{\Psi}_{m,m+1} = \operatorname{diag}\{e^{j\psi_i}\}$. Right-multiplication of $\boldsymbol{V}_m$ by this matrix provides the aforementioned parameterization. Second, the ordering of the eigenpairs may vary from one sample to the next, and this ordering is also unknown. We take this into consideration by defining an unknown permutation matrix $\boldsymbol{P}_{m,m+1}$ having a single unitary entry in each row and column. Right-multiplication by this matrix provides a columnwise permutation. As a result, we have the following representation:

$$\boldsymbol{V}_{m+1} = \boldsymbol{V}_m \boldsymbol{\Psi}_{m,m+1} \boldsymbol{P}_{m,m+1} + \delta\boldsymbol{V}_{m,m+1} \tag{16}$$

where the first term is the eigenvector matrix at sample m, whose columns are phase-shifted and permuted. The following derivation allows to estimate the phase shifts $\boldsymbol{\Psi}_{m,m+1}$ and the permutation matrix $\boldsymbol{P}_{m,m+1}$ that are necessary to "adapt" the eigenvector matrix $\boldsymbol{V}_m$ according to the ordering and to the phases of the eigenvectors at sample $m+1$. As a result, it will be possible to regard the second term in (16) as a true (complex) perturbation, independent of phase shifts and ordering. Our final aim is to determine whether this perturbation $\delta\boldsymbol{V}_{m,m+1}$ on the eigenvectors is small. We compute therefore the mutual product

$$\begin{aligned}\widetilde{\boldsymbol{P}}_{m,m+1} &= \boldsymbol{V}_m^H \boldsymbol{V}_{m+1} \\ &= \boldsymbol{\Psi}_{m,m+1}\boldsymbol{P}_{m,m+1} + \boldsymbol{V}_m^H \delta\boldsymbol{V}_{m,m+1}. \end{aligned} \quad (17)$$

In case of accurate sampling, the matrix $\widetilde{\boldsymbol{P}}_{m,m+1}$ is a good approximation of a true permutation matrix, up to arbitrary phase terms. We attempt the recovering of the true permutation matrix by computing

$$\widehat{\boldsymbol{P}}_{m,m+1} = \mathcal{I}\left(|\widetilde{\boldsymbol{P}}_{m,m+1}|\right) \quad (18)$$

where the operator $\mathcal{I}(\cdot)$ rounds towards the nearest integer its matrix argument and the absolute value is taken componentwise. Note that, in case of negligible perturbations $\delta\boldsymbol{V}_{m,m+1}$, this absolute value allows to get rid of the arbitrary phase terms, which are cancelled out. In general, two cases may apply. If $\widehat{\boldsymbol{P}}_{m,m+1}$ is a malformed permutation matrix, the amount of perturbation in the eigenvectors from sample m to sample $m+1$ is too large, and no tracking can be performed. This implies that also the eigenvalues at sample $m+1$ cannot be regarded as small perturbations of those at sample m. There will be no guarantee of accuracy within the considered frequency interval, which is flagged and will be refined at next iteration. If instead the result is a valid permutation matrix, it can be inferred that eigenvectors can be tracked from sample m to sample $m+1$. The individual eigenvalues at sample $m+1$ will also be small perturbations of those at sample m, and no refinement of this frequency interval is needed. In order to validate this assumption, we compute the product

$$\begin{aligned}\boldsymbol{J}_{m,m+1} &= \widehat{\boldsymbol{P}}_{m,m+1}^T \widetilde{\boldsymbol{P}}_{m,m+1} \\ &= \widehat{\boldsymbol{P}}_{m,m+1}^T \boldsymbol{\Psi}_{m,m+1}\boldsymbol{P}_{m,m+1} \\ &\quad + \widehat{\boldsymbol{P}}_{m,m+1}^T \boldsymbol{V}_m^H \delta\boldsymbol{V}_{m,m+1}. \end{aligned}$$

If the estimate $\widehat{\boldsymbol{P}}_{m,m+1}$ is correct, matrix $\boldsymbol{J}_{m,m+1}$ is a small perturbation of a phase-shifted identity matrix (showing the effect of a correct reordering of the eigenvectors), with the perturbation terms being the components of $\delta\boldsymbol{V}_{m,m+1}$ with respect to the reordered eigenvectors at sample m. The frequency interval is accepted as accurate when the simple estimate on the amount of perturbation

$$\max_{i,i'} \left\{ \left| \left(|\boldsymbol{J}_{m,m+1}| - \boldsymbol{I} \right) \right|_{i,i'} \right\} < \varepsilon \quad (19)$$

is satisfied for a sufficiently small threshold ε (the absolute values always being taken componentwise). We use in this work $\varepsilon = 0.2$. If this is not the case, the interval is flagged as inaccurate and it will be refined at the next iteration. An illustrative plot of the perturbation estimate in (19) is provided in Fig. 2 for a test case (denoted as Case III in Section V). Note that in the bottom panel, corresponding to the final result of the adaptive sampling process, the perturbation estimates between any pair of adjacent samples are uniformly bounded by the adopted threshold.

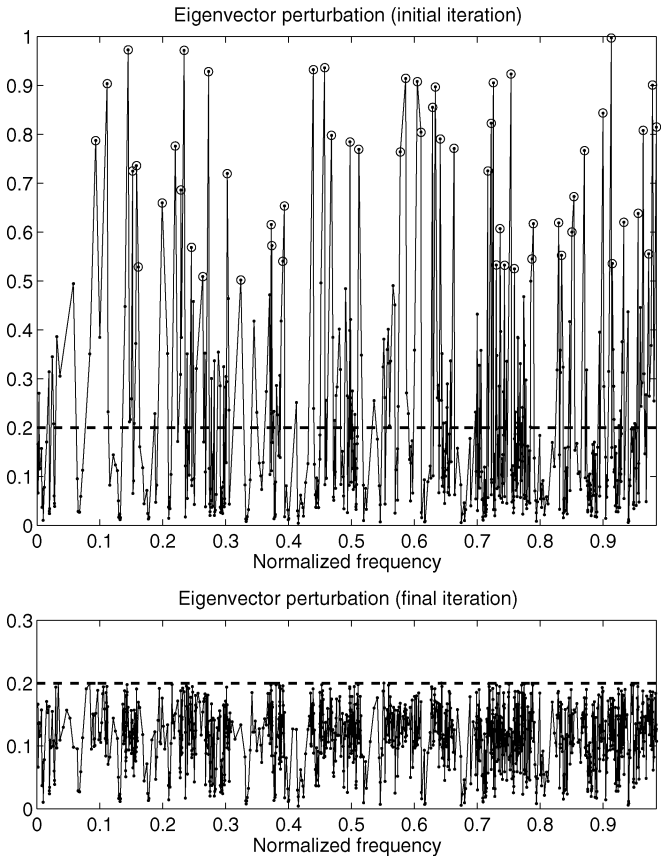

Fig. 2. Eigenvector perturbation defined as in (19) at initial (top) and final (bottom) iterations of the adaptive sampling process. Big circles in the top panel indicate the frequency samples associated with incorrectly formed permutation matrices.

Iterative refinement is achieved by inserting an additional frequency sample at the midpoint of each flagged interval, and by repeating the above checks only on the newly generated intervals. The above procedure is very simple and straightforward, yet it allows to track the frequency dependence of individual eigenvalues λ_i even if they cross each other between any pair of frequency samples. Eigenvector tracking is essential in this case, since the computed permutation matrix allows to establish a one-to-one correspondence between the eigenvalues at the two frequencies, independent on the ordering obtained from the adopted eigensolver. Fig. 3 shows a snapshot of the initial and final sampling of the eigenvalues $\lambda_i(j\omega)$ for the same test case used in Fig. 2. Although the initial sampling is already quite representative of the significant frequency variations, the final sampling allows tracking of each eigenvalue throughout the frequency band of interest.

The only case when the procedure may break down occurs in case of multiple eigenvalues. In this case, even though the invariant subspace associated to the multiple eigenvalue is well

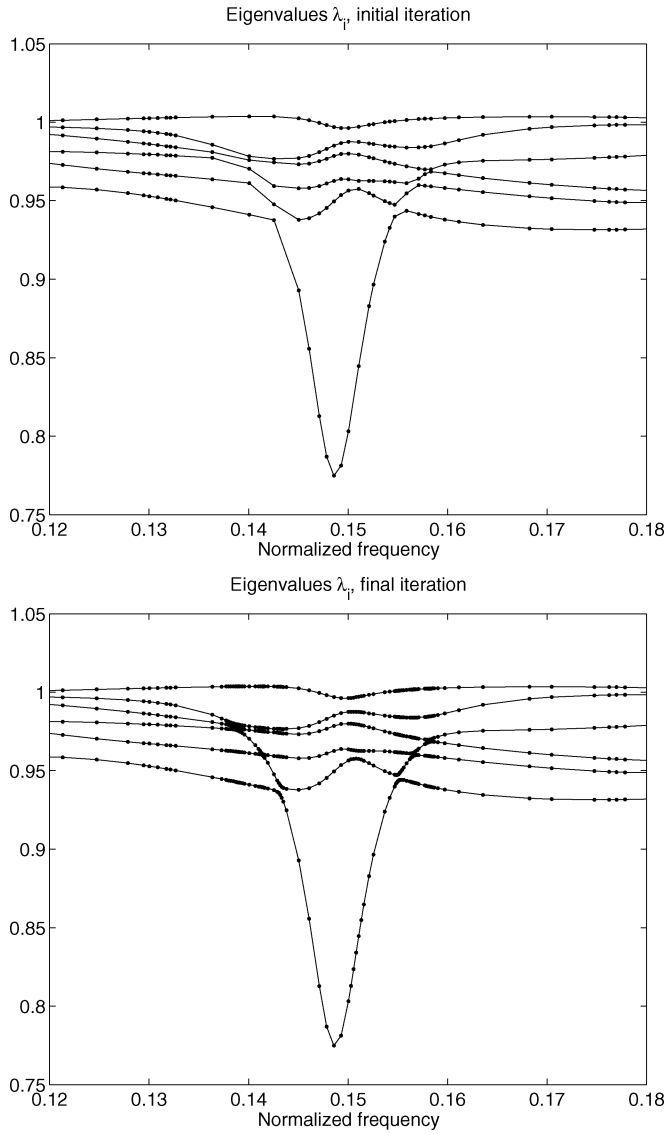

Fig. 3. Spectrum of eigenvalues $\lambda_i(j\omega)$ at the initial and final iterations of the adaptive sampling process for an illustrative case.

determined, the actual basis of eigenvectors for this invariant subspace is not unique, depending on the eigensolution algorithm and in some cases even on different runs of the same algorithm. Therefore, a correct permutation matrix will never be obtained by (18). However, this case is easily detectable, e.g., when

$$\max_{i,i'} |\lambda_i(j\omega_m) - \lambda_{i'}(j\omega_m)| < k\epsilon \max_i |\lambda_i(j\omega_m)| \qquad (20)$$

where ϵ is the machine precision and $k > 1$ is a small constant. Since the occurrence of multiple eigenvalues is not structurally stable with respect to the small variations of the frequency, the above condition will not be satisfied at samples $m-1$ and $m+1$. Therefore, it is sufficient to eliminate the critical frequency sample m whenever (20) is satisfied during the refinement iterations. The left and right neighbors will guarantee both eigenvector and eigenvalue tracking even through the crossing point. Fig. 4 provides a graphical illustration for a simple 2×2 test case with eigenvalues and eigenvectors expressed as

$$\lambda_{1,2} = 1 \pm 0.9\sin(\pi x/2)$$
$$\boldsymbol{V} = \begin{pmatrix} \cos(x-a) & \sin(x-a) \\ -\sin(x-a) & \cos(x-a) \end{pmatrix}.$$

D. Detection of Strictly Passive Frequency Bands

In this section, we illustrate a procedure for the determination of the strictly passive frequency bands of (6) and (7). Since these passivity conditions must be satisfied for any $\omega \in \Omega_q$, care must be taken in drawing such conclusions only from a set of discrete samples. Indeed, there is no *a priori* guarantee that the passivity threshold $\gamma = 1$ will not be exceeded at some frequency that was missed during the sampling process. This becomes critical when one or more eigenvalues λ_i become close to the threshold. In this case, it may be difficult to infer whether there is a potential passivity violation using hard thresholding. We show in the following how the procedure of Sections III-B and III-C allows to handle these difficulties.

We recall that the eigenvector tracking procedure of Section III-C leads to a set of accuracy-controlled frequency samples. At each sample ω_m, the eigenvalues $\boldsymbol{\Lambda}_m$ and the eigenvectors $\boldsymbol{V}_m$ are known. Since also the permutation matrices allowing to track each eigenvalue at different frequencies have been derived, we will assume in the following that the eigenpairs have been reordered so that each $\lambda_i(j\omega)$ for fixed i is a continuous and differentiable curve versus frequency. This fact is essential for the detection of the strictly passive bandwidths, which is detailed next. Under these assumptions, we can safely assume that

$$\begin{aligned} \boldsymbol{\Theta}_{m+1} &= \boldsymbol{\Theta}_m + \delta\boldsymbol{\Theta}_{m,m+1} \\ \boldsymbol{V}_{m+1} &= \boldsymbol{V}_m + \delta\boldsymbol{V}_{m,m+1} \\ \boldsymbol{\Lambda}_{m+1} &= \boldsymbol{\Lambda}_m + \delta\boldsymbol{\Lambda}_{m,m+1} \end{aligned} \qquad (21)$$

where the various perturbation terms are small. This enables us to provide first-order estimates of the eigenvalues $\boldsymbol{\Lambda}_{m+1}$ starting from the adjacent sample m.

At least two different first-order estimates for the eigenvalues at sample $m+1$ can be computed. The first one uses the eigenvectors at sample m and the known perturbation $\delta\boldsymbol{\Theta}_m$. We have

$$\boldsymbol{\Lambda}'_{m+1} = \boldsymbol{\Lambda}_m + \boldsymbol{V}_m^H \delta\boldsymbol{\Theta}_{m,m+1} \boldsymbol{V}_m = \boldsymbol{V}_m^H \boldsymbol{\Theta}_{m+1} \boldsymbol{V}_m \qquad (22)$$

Since the exact eigenvalues $\boldsymbol{\Lambda}_{m+1}$ are also known, we can associate a prediction error, expressed as

$$\Delta_{m+1} = \max_i \left\{ \left| \left(\boldsymbol{\Lambda}'_{m+1}\right)_{ii} - \left(\boldsymbol{\Lambda}_{m+1}\right)_{ii} \right| \right\}. \qquad (23)$$

The interval (ω_m, ω_{m+1}) is concluded to be passive, with all eigenvalues less than the threshold $\gamma = 1$, when

$$\gamma - \max_i \{\lambda_i(j\omega_{m+1})\} > \beta\Delta_{m+1}, \qquad (24)$$

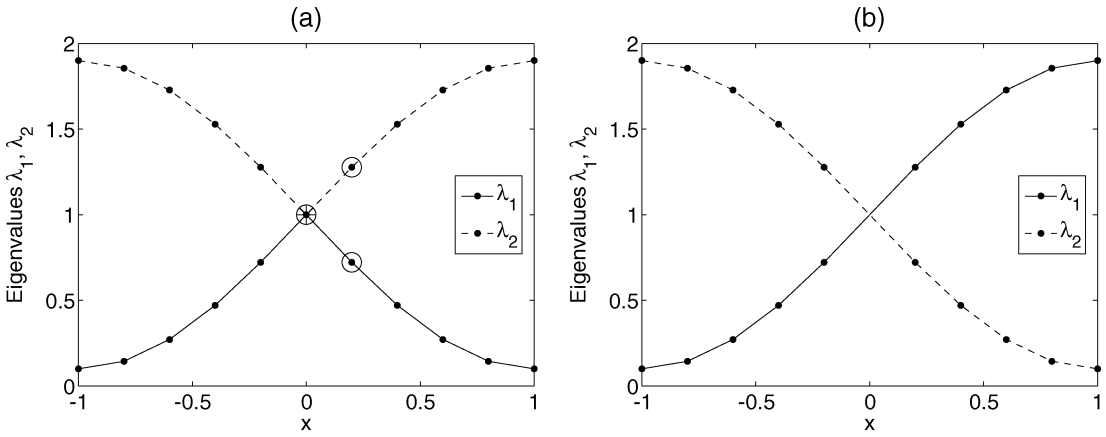

Fig. 4. Handling multiple eigenvalues. Panel (a) reports the two coarsely sampled eigenvalues $\lambda_{1,2}$ including a sample at $x = 0$ (highlighted by a star) where $\lambda_1 = \lambda_2$. Circles correspond to malformed permutation matrices, computed as in Section III-C. Skipping the critical sample $x = 0$ in panel (b) leads to a correct numerical identification and tracking of each eigenvalue.

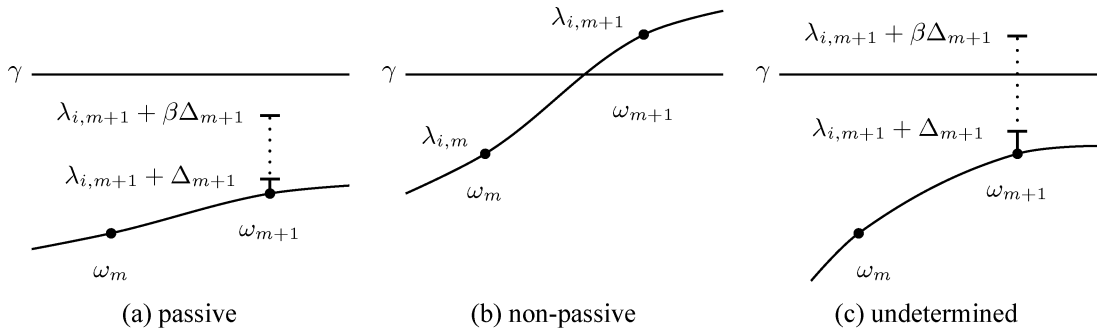

Fig. 5. Classification of passive intervals (left) satisfying (24) and non-passive intervals (middle) satisfying (25). All other intervals (right) are characterized by eigenvalues that are too close to the threshold to be classified based on the frequency sampling test only.

where β is a suitable safety factor. In this work, we used $\beta = 5$ in all numerical tests. It is important to note that condition (24) parameterizes how close can an eigenvalue $\lambda_i(j\omega_{m+1})$ is to the threshold in terms of its maximum prediction error Δ_{m+1}, as depicted in Fig. 5. Detection of strictly nonpassive intervals is straightforward, since it is sufficient to test the maximum eigenvalue at both edges via

$$\max_i \{\lambda_i(j\omega_m), \lambda_i(j\omega_{m+1})\} > \gamma. \tag{25}$$

When both conditions (24) and (25) are not satisfied, no conclusions can be drawn on the actual passivity or non-passivity within the corresponding interval, since the largest eigenvalue is too close to the threshold (see Fig. 5). This interval must be flagged as "suspect passivity violation" and must be checked by a more precise test, to be presented in Section IV.

An alternative estimate for the prediction error on each eigenvalue can be obtained by applying linearization to each curve $\lambda_i(j\omega)$. This is accomplished by the following steps. First, the frequency derivative of the transfer matrix (2) is computed at each available sample as

$$\boldsymbol{H}'_m = \left.\frac{d\boldsymbol{H}}{d\omega}\right|_{\omega_m} = -j\boldsymbol{C}(j\omega_m\boldsymbol{I} - \boldsymbol{A})^{-2}\boldsymbol{B}. \tag{26}$$

This is used to derive a first-order expansion of $\boldsymbol{\Theta}(j\omega)$ around ω_m, which reads

$$\begin{aligned}\boldsymbol{\Theta}(j\omega) \sim &\boldsymbol{\Theta}_m + (\omega - \omega_m)\left\{\boldsymbol{H}'^H_m\boldsymbol{H}_m + \boldsymbol{H}^H_m\boldsymbol{H}'_m\right\} \\ = &\boldsymbol{\Theta}_m + (\omega - \omega_m)\boldsymbol{\Theta}'_m.\end{aligned} \tag{27}$$

Finally, the frequency-dependent linearizations of the eigenvalues around ω_m is obtained from the diagonal entries of

$$\boldsymbol{\Lambda}''_{m+1} = \boldsymbol{\Lambda}_m + (\omega - \omega_m)\boldsymbol{V}^H_m\boldsymbol{\Theta}'_m\boldsymbol{V}_m. \tag{28}$$

This estimate can be used as above in (23) to compute an alternative linear prediction error for the determination of the strictly passive intervals. Very similar results were obtained by the two estimates (22) and (28). Therefore, we report in this work only results based on the estimate (22), which allows to save the extra computations in (26) and (27) required by the eigenvalues linearization process.

A remark on a possible situation that may lead to a failure of the proposed test. It is conceivable that the transfer matrix $\boldsymbol{H}(j\omega)$ exhibits a limited periodic behavior. This implies that, in case two of the initial samples are displaced by exactly one period, all eigenpairs will be identical at the two samples, with practicaly no perturbation. The linear prediction error will also

be negligible, and (24) will be satisfied without any real connection to the actual behavior of the eigenvalues inbetween the two samples. This in turn may flag as strictly passive a frequency band that is instead "suspect." However, the proposed definition of the poles-dependent initial set of frequency samples (see Section III-B) is very likely to rule out this situation, which is indeed extremely rare and was never observed in our numerical tests.

To summarize, after checking all the frequency intervals arising from the adaptive sampling process, we obtain the following decomposition

$$\begin{aligned} \Omega^{\text{passive}} \cup \Omega^{\text{suspect}} &= [0, \omega_{\max}] \\ \Omega^{\text{passive}} \cap \Omega^{\text{suspect}} &= \emptyset \end{aligned} \tag{29}$$

where the "suspect" frequency bands

$$\Omega^{\text{suspect}} = \bigcup_{q=1}^{Q'} [\omega'_{q,0}, \omega'_{q,1}] \tag{30}$$

include both non-passive and undetermined intervals. Imaginary Hamiltonian eigenvalues can indeed be located in any of these intervals, which will need further checking, in order to resolve the ambiguity arising from the finite size of the considered frequency samples. Fig. 6 depicts the results of the proposed identification of the passive bandwidths Ω^{passive} for the test case under consideration. Note that, due to the adaptive sampling process, quite accurate estimates of the maximum passivity violation amounts, i.e., the maxima reached by the singular values in each "suspect" frequency band, are available. These are also highlighted in the plot. We conclude this section by noting that the complete adaptive sampling scheme has a computational cost that scales quadratically as $O(N^2)$ with the macromodel size, since the cost per sample is $O(N)$ and the number of samples is also proportional to N.

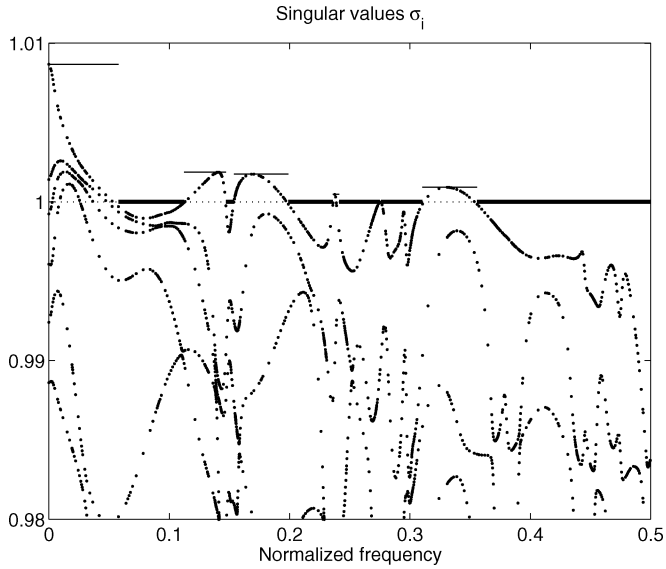

Fig. 6. Detection of passive frequency intervals Ω^{passive}, highlighted by thick lines at the singular value threshold $\gamma = 1$. The "suspect" frequency bands are depicted by a thin dashed line, with the corresponding maximum passivity violation amount being highlighted by a continuous thin line. The dots are the available samples of the singular values σ_i.

IV. Imaginary Eigenvalues and Passivity Enforcement

We give here a brief outline of the complete algorithm for the identification of all imaginary eigenvalues of the Hamiltonian matrix (5). The main steps of the proposed scheme are listed in Algorithm 1. Note that steps 1–8 are just a summary of Sections III-A–III-C and do not need additional comments. The result of step 8 is a set of strictly passive disjoint frequency bands Ω^{passive}, which do not need to be processed any further. These intervals are highlighted by thick lines in Figs. 1 and 6.

The loop in steps 9–12 is performed over the finite number Q' of disjoint subintervals $[\omega'_{q,0}, \omega'_{q,1}]$ that could not be classified as strictly passive during the adaptive sampling process. The computation of the imaginary eigenvalues of the Hamiltonian matrix restricted to each subinterval is performed at line 10. The algorithm that is employed here has already been described in full detail in [26] and [35] and is not repeated here. We only recall that a bisection process is started by placing two shifts $j\omega'_{q,0}$ and $j\omega'_{q,1}$ at the edges of the interval. A restarted Arnoldi process is run at each shift in order to compute the closest eigenvalues of the Hamiltonian matrix. The converging eigenvalue which is furthest to the shift also determines a convergence circle (see Fig. 1 for a graphical illustration), insuring that all eigenvalues within the circle are found. If the collection of convergence circles cover entirely the interval $[\omega'_{q,0}, \omega'_{q,1}]$, it is guaranteed that all imaginary eigenvalues within the latter have been found. Otherwise, new shifts $j\omega_{q,\tau}$ are placed in the midpoints of each uncovered portion of the interval and the scheme is iterated until completion. We remark that the computational cost for this determination scales only linearly with the number of macromodel states. See [26] and [35] for details. Further optimizations and enhancements could be provided by structured

Algorithm 1 Find all imaginary eigenvalues $\mathcal{S} = \{j\omega_k\}$ of Hamiltonian matrix $\mathcal{M}$ of (5).

Require: state-space matrices $\boldsymbol{A}$, $\boldsymbol{B}$, $\boldsymbol{C}$, $\boldsymbol{D}$

1: compute the upper bound $\omega_{\max}$ for all Hamiltonian eigenvalues as in Section III-A
2: generate a set of initial M samples based on the poles distribution, as in Section III-B
3: **while** $M > 0$ **do**
4: compute and store $\boldsymbol{\Theta}_m$, $\boldsymbol{V}_m$, $\boldsymbol{\Lambda}_m$ for $m = 1, \ldots, M$ as in Section III-C
5: estimate eigenvector perturbations via (19) and identify frequency intervals to be refined
6: redefine M as number of new required samples
7: **end while**
8: compute Ω^{passive} and Ω^{suspect} based on (6), (24), and (30)
9: **for** $q = 1, \ldots, Q'$ **do**
10: perform a multishift bisection process [26], [35] on each sub-interval $[\omega'_{q,0}, \omega'_{q,1}] \in \Omega^{\text{suspect}}$
11: collect the detected imaginary eigenvalues in $\mathcal{S}_q$
12: collect the maximum violation amounts in $\sigma^q_{\max}$, as depicted in Fig. 6
13: **end for**
14: collect all subsets of imaginary eigenvalues $\mathcal{S} = \cup_q \mathcal{S}_q$

Arnoldi methods exploiting the symmetry of the Hamiltonian eigenspectrum [42], which were not investigated here.

The maximum singular value $\sigma^q_{\max}$ within each of the "suspect" frequency bands is readily estimated by searching the maximum among the finite number of available samples, as discussed in Section III-D. Although this estimate can be refined to arbitrary precision by applying the techniques of [20] and [25], this is carefully avoided here. In fact, these techniques require additional determinations of the Hamiltonian eigenspectrum, which in turn increase the computational cost. Since these maxima are only used by the passivity compensation scheme for the automatic displacement of the imaginary Hamiltonian eigenvalues, their estimate do not need to be extremely precise. The above considerations allow an extra speedup of the overall passivity enforcement scheme.

We conclude this section by recalling the main passivity enforcement scheme, fully documented in [21] and [25]. The computed imaginary eigenvalues of the Hamiltonian matrix pinpoint the frequencies at which the singular value curves touch or cross the passivity threshold $\gamma = 1$. The associated left and right eigenvectors, which are also known as a byproduct at the end of the Arnoldi iterations, are used to linearize the frequency-dependent singular values at the crossing points. The slopes of these linearizations lead to a precise determination of the true bandwidths where passivity violations occur. Note that these cannot be estimated by Algorithm 1 with sufficient confidence level. The slopes and the maxima $\sigma^q_{\max}$ are then employed as in [25] to predict suitable relocations of the imaginary eigenvalues allowing to reduce the size of the passivity violation intervals. The actual displacement is performed by computing a modified state matrix $\tilde{\boldsymbol{C}}$ corresponding to the above relocations, based on linear perturbation theory. This results in a small underdetermined linear system having a row count identical to the number of imaginary eigenvalues to be solved. The accuracy of the initial macromodel is preserved by enforcing the technical condition

$$\min \operatorname{Tr}\left\{(\tilde{\boldsymbol{C}} - \boldsymbol{C})\boldsymbol{W}(\tilde{\boldsymbol{C}} - \boldsymbol{C})^T\right\} \tag{31}$$

during the solution of this system, where $\boldsymbol{W}$ is the controllability Gramian associated to the macromodel. The procedure is iterated, until all imaginary eigenvaules have been removed and therefore until the perturbed macromodel is passive. All details are available in [25] and [26].

V. Numerical Results

The performance of the proposed methodology is demonstrated on a large number of test cases, summarized in Table I. Each case is a macromodel derived from frequency tables of scattering matrices obtained by full-wave electromagnetic simulations. Each model in the table was derived by computing a rational approximation of the scattering matrix entries via the macromodeling software `IdEM` [43], which is based on various formulations of the well-known vector fitting algorithm [8]. All models refer to interconnect structures commonly found in any high-speed electronic system, and are grouped in Table I by interconnect type. In particular, cases I and II are high-speed packaging structures (courtesy of Sigrity, Inc., Santa Clara, CA). These two cases were already thoroughly analyzed in [26] and [35]. Case III is a model of a 6-port interconnected system including two power/ground conductors (ports 1 and 2), and two signal conductors, terminated by ports 3–6. See [28] for a detailed description of the geometry. Cases IV and V are two macromodels of a 20-port via field under an LGA connector (courtesy of IBM). These two models differ only for the number of poles that were used in the rational approximation (see also [26]). Cases VI–VIII represent different 3×3 sections of a high-speed card-board connector over a bandwidth of 20 GHz (courtesy of IBM). Case IX is a 12-port section of a DIMM connector, inclusive of suitable segments of power/ground planes, vias, signal lines, and pads (courtesy of IBM). Finally, cases X–XIII represent various configurations of 3×3 via fields (courtesy of IBM). We remark that results from previous implementations of the passivity compensation scheme for the first six cases have been published elsewhere (see, e.g., [26] and [27]). These cases are included in this report in order to show the significant improvements that were achieved with the new proposed algorithm. All other cases are new. We also note that all computations have been repeated here on the same computer platform, namely a Pentium IV-based PC with a 3-GHz clock under a MATLAB R14 [41] environment, in order to allow relative comparison between various models. This explains some differences in the CPU times herewith reported with respect to previously published results.

TABLE I
Benchmark Macromodels Used for All Numerical Tests

Model	Poles N	Ports P	Description
Case I	820	10	Package interconnect
Case II	1488	12	Package interconnect
Case III	450	6	Signal/Power bus
Case IV	600	20	LGA via field
Case V	1000	20	LGA via field
Case VI	1368	18	Connector
Case VII	1616	18	Connector
Case VIII	1368	18	Connector
Case IX	720	12	Connector
Case X	468	18	Via field
Case XI	646	18	Via field
Case XII	646	18	Via field
Case XIII	684	18	Via field

The adaptive sampling strategy presented in this work removes essentially the main limitation of existing Hamiltonian-based passivity check and compensation algorithms, namely, the excessive computation time required by the determination of the Hamiltonian eigenvalues. Table II shows the CPU time required by the extraction of the imaginary Hamiltonian eigenvalues associated to each macromodel in Table I. The column labeled with "CFH (full)" reports the CPU time required by the CFH-based sweep over the full bandwidth, without using the adaptive sampling scheme. This is the algorithm that was documented in [26] and [35]. The column labeled with "CFH (adaptive)" reports the same CPU time obtained by the new presented algorithm based on adaptive sampling combined with separate CFH runs on the reduced-size "suspect" subbands. The speedup factor is also reported, together with the maximum relative deviation among all pairs of detected eigenvalues. We remark that

TABLE II
CPU TIME REQUIRED BY THE COMPUTATION OF THE IMAGINARY EIGENVALUES OF THE HAMILTONIAN MATRIX. SEE TEXT FOR DETAILS. ALL COMPUTATIONS WERE PERFORMED WITH A PENTIUM IV (3.0 GHz) PC

Model	CFH (full)	CFH (adaptive)	Speedup	Max deviation
Case I	48 sec	3.7 sec	13	1.8×10^{-15}
Case II	26 sec	17 sec	1.5	2.8×10^{-14}
Case III	30 sec	8.1 sec	3.7	1.1×10^{-14}
Case IV	46 sec	18 sec	2.5	2.8×10^{-14}
Case V	160 sec	26 sec	6	3.6×10^{-15}
Case VI	420 sec	41 sec	10	2.2×10^{-14}
Case VII	685 sec	51 sec	13	1.6×10^{-14}
Case VIII	476 sec	48 sec	10	1.4×10^{-14}
Case IX	38 sec	12 sec	3.0	4.0×10^{-14}
Case X	13 sec	16 sec	0.8	9.5×10^{-14}
Case XI	72 sec	15 sec	4.7	1.2×10^{-14}
Case XII	72 sec	14 sec	4.9	4.2×10^{-15}
Case XIII	59 sec	17 sec	3.4	2.8×10^{-14}

TABLE III
CPU TIME REQUIRED BY THE PASSIVITY COMPENSATION SCHEMES APPLIED TO THE TEST CASES OF TABLE I; T_A: FULL EIGENSOLVER; T_B: CFH APPLIED TO THE ENTIRE BANDWIDTH; T_C: CFH COMBINED WITH ADAPTIVE SAMPLING. THE SPEEDUP FACTORS ACHIEVED BY THE PROPOSED METHOD ARE ALSO REPORTED IN THE LAST TWO COLUMNS. ALL COMPUTATIONS WERE PERFORMED WITH A PENTIUM IV (3.0 GHz) PC

Model	Iterations	T_A	T_B	T_C	T_A/T_C	T_B/T_C
Case I	9	30 min	7.0 min	34 sec	51	12
Case II	13	8.3 hrs	8.9 min	2.8 min	174	3.1
Case III	13	16 min	6.6 min	1.4 min	11	4.7
Case IV	20	36 min	14 min	4.6 min	7.8	3.0
Case V	13	77 min	35 min	5.3 min	15	6.6
Case VI	7	96 min	58 min	4.5 min	21	13
Case VII	18	14 hrs	4.1 hrs	15 min	55	16
Case VIII	9	111 min	40 min	7.4 min	15	5.4
Case IX	23	105 min	22 min	5.5 min	19	4.1
Case X	27	43 min	17 min	5.8 min	7.5	2.9
Case XI	23	128 min	31 min	8.3 min	15	3.7
Case XII	23	116 min	29 min	8.0 min	14	3.6
Case XIII	22	61 min	25 min	7.3 min	8.3	3.4

the same imaginary eigenvalues were detected by the two algorithms for all cases. As expected, higher speedup factors are obtained for larger models. For models with similar size, the best speedup occurs when the number of ports is small. This is obviously due to the fact that the computational cost of the adaptive sampling scheme scales as the third power of the number of ports P. For Case X, this overhead becomes comparable to the actual eigenvalue computation time. We remark that the CPU times reported in the "CFH (adaptive)" column are practically coincident with the CPU time required for the global passivity check of each macromodel.

The main objective of this paper is to speed up existing formulations of global passivity enforcement schemes based on Hamiltonian eigenvalues. Therefore, we applied three different implementations of such passivity enforcement methods to all macromodels of Table I, reporting the results in Table III. The CPU times in the table are defined as follows.

T_A This column reports the CPU time required by the standard passivity compensation scheme based on a full general-purpose eigensolver. This scheme was first documented in [25].

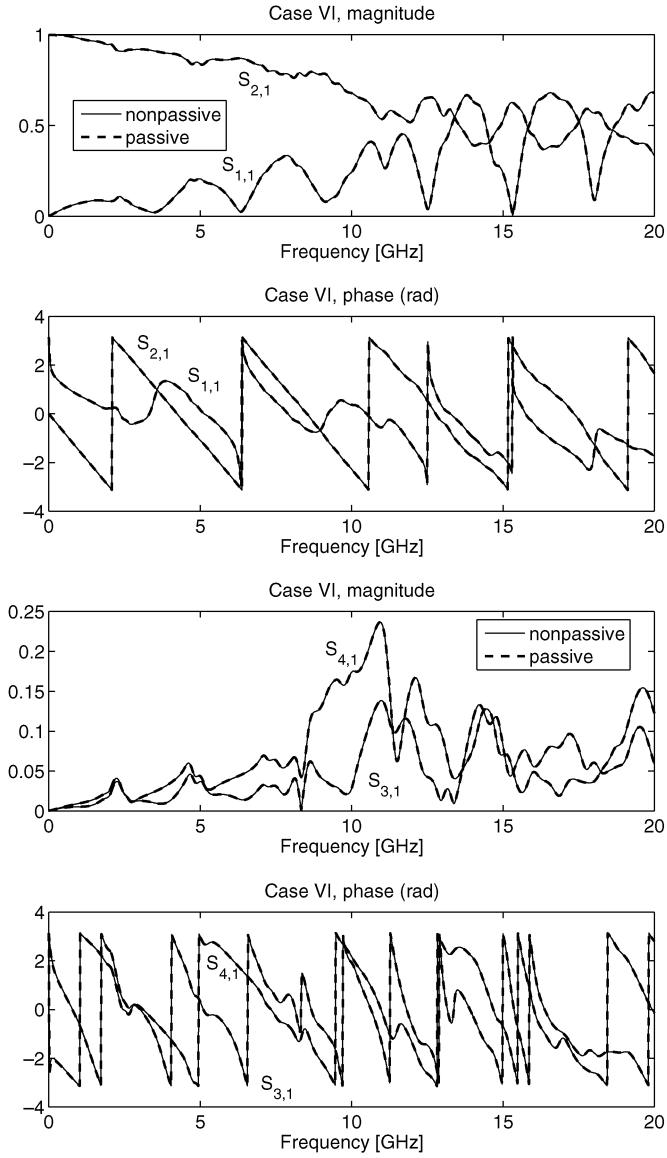

Fig. 7. Comparison of Case VI macromodels before and after passivity compensation. Some significant scattering responses before and after passivity compensation are reported in both magnitude and phase.

T_B This is the CPU time required by the passivity enforcement scheme described in [26], [35]. The Hamiltonian eigenspectrum is computed via CFH application to the entire bandwidth, without employing any preprocessing step.

T_C This is the CPU time required by the scheme proposed in this paper and based on a mixed adaptive sampling/CFH application for the determination of the Hamiltonian eigenvalues.

The speedup factors of the new algorithm with respect to the other two implementations are also reported in the last two columns. These results confirm that the proposed scheme leads to a quite efficient passivity compensation even for the most critical cases, for which the introduction of a sparse decomposition of the Hamiltonian matrix in [26] was not effective. The compensation is achieved in few minutes for all cases, thus showing significant potential for its automated application to

complex multiport interconnect models characterized by a large dynamic order. Note also that all different implementations of the compensation scheme lead to identical results (and require the same number of iterations), since the only differences are in the actual routine that performs the identification of the imaginary eigenvalues.

We complete the presentation by comparing in Fig. 7 a few representative scattering responses of the passive models to the corresponding ones of the nonpassive models before applying the compensation scheme. We only report results for Case VI, since Cases I–V have been documented in [26], and identical conclusions hold for all other cases. The deviation between passive and non-passive models is hardly visible. This confirms that the passivity compensation is performed without compromising the accuracy, and that no overtreatment occurs.

VI. Conclusion

A new accuracy-controlled adaptive sampling scheme is proposed in this paper. The scheme allows to track continuously throughout an automatically determined bandwidth the variation of individual eigenvalues (singular values) and eigenvectors (singular vectors) of a given transfer matrix associated to a rational macromodel. This tracking is used in turn to speed up the computation of purely imaginary eigenvalues of the Hamiltonian matrix associated to the macromodel, thus enabling a fast enforcement of the global macromodel passivity over the full frequency spectrum. The numerical results provided for an extensive set of models representing various interconnect structures show a very weak dependence of the computational cost with respect to the macromodel size. In other words, the proposed scheme removes the main limitation of existing passivity compensation schemes based on Hamiltonian eigenvalues, and enables their systematic application in practical computer-aided design environments for analysis and design of high-speed interconnected systems.

Acknowledgment

The author would like to thank J. Zheng (Sigrity, Inc.), E. Klink, D. Kaller, L. Shan, A. Deutsch, E. Genovese, and M. Bandinu (IBM) for providing some of the test cases that were used in this paper.

References

[1] W. Beyene and J. Schutt-Ainé, "Accurate frequency-domain modeling and efficient circuit simulation of high-speed packaging interconnects," *IEEE Trans. Microwave Theory Tech.*, vol. 45, no. 10, pp. 1941–1947, Oct. 1997.

[2] K. L. Choi and M. Swaminathan, "Development of model libraries for embedded passives using network synthesis," *IEEE Trans. Circuits Syst. II Exp. Briefs*, vol. 47, no. 4, pp. 249–260, Apr. 2000.

[3] W. Do Couto Boaventura, A. Semlyen, M. Reza Iravani, and A. Lopes, "Sparse network equivalent based on time-domain fitting," *IEEE Trans. Power Del.*, vol. 17, no. 1, pp. 182–189, Jan. 2002.

[4] M. Elzinga, K. Virga, L. Zhao, and J. L. Prince, "Pole-residue formulation for transient simulation of high-frequency interconnects using householder LS curve-fitting techniques," *IEEE Trans. Comp. Packag. Manufact. Technol.*, vol. 23, no. 2, pp. 142–147, Mar. 2000.

[5] M. Elzinga, K. Virga, and J. L. Prince, "Improve global rational approximation macromodeling algorithm for networks characterized by frequency-sampled data," *IEEE Trans. Microwave Theory Tech.*, vol. 48, no. 9, pp. 1461–1467, Sep. 2000.

[6] S. Grivet-Talocia, F. Canavero, I. Maio, and I. Stievano, "Reduced-order macromodeling of complex multiport interconnects," in *URSI General Assembly*, Maastricht, Belgium, Aug. 19–23, 2002.

[7] S. Grivet-Talocia, "Package macromodeling via time-domain vector fitting," *IEEE Microwave Wireless Comp. Lett.*, vol. 13, no. 11, pp. 472–474, Nov. 2003.

[8] B. Gustavsen and A. Semlyen, "Rational approximation of frequency responses by vector fitting," *IEEE Trans. Power Del.*, vol. 14, no. 3, pp. 1052–1061, Jul. 1999.

[9] S. Grivet-Talocia, "Passive time-domain macromodeling of large complex interconnects," presented at the 20th Annu. Rev. Progress Appl. Computational Electromagn. (ACES04), Syracuse, NY, Apr. 19–23, 2004.

[10] S. Grivet-Talocia, F. G. Canavero, I. S. Stievano, and I. A. Maio, "Circuit extraction via time-domain vector fitting," presented at the 2004 IEEE Symp. EMC, Santa Clara, CA, Aug. 9–13, 2004.

[11] M. Celik, L. Pileggi, and A. Obadasioglu, *IC Interconnect Analysis*. Norwell, MA: Kluwer, 2002.

[12] M. Nakhla and R. Achar, "Simulation of high-speed interconnects," *Proc. IEEE*, vol. 89, no. 5, pp. 693–728, May 2001.

[13] V. Belevitch, *Classical Network Theory*. San Francisco: Holden-Day, 1968.

[14] K. Zhou, J. C. Doyle, and K. Glover, *Robust and Optimal Control*. New York: Prentice Hall, 1996.

[15] J. Morsey and A. C. Cangellaris, "PRIME: Passive realization of interconnects models from measures data," in *Proc. IEEE 10th Topical Meeting Electr. Perf. Electron. Packag.*, Oct. 2001, pp. 47–50.

[16] B. Gustavsen and A. Semlyen, "Enforcing passivity for admittance matrices approximated by rational functions," *IEEE Trans. Power Syst.*, vol. 16, no. 1, pp. 97–104, Feb. 2001.

[17] C. P. Coelho, J. Phillips, and L. M. Silveira, "A convex programming approach for generating guaranteed passive approximations to tabulated frequency-data," *IEEE Trans. Computed-Aided Design Integr. Circuits Syst.*, vol. 23, no. 2, pp. 293–301, Feb. 2004.

[18] S. Boyd, L. El Ghaoui, E. Feron, and V. Balakrishnan, *Linear Matrix Inequalities in System and Control Theory, SIAM Studies in Applied Mathematics*. Philadelphia, PA: SIAM, 1994.

[19] H. Chen and J. Fang, "Enforcing bounded realness of S parameter through trace parameterization," in *12th IEEE Topical Meeting Electrical Performance Electronic Packag.*, Princeton, NJ, Oct. 27–29, 2003, pp. 291–294.

[20] S. Boyd, V. Balakrishnan, and P. Kabamba, "A bisection method for computing the H_∞ norm of a transfer matrix and related problems," *Math. Control Signals Syst.*, vol. 2, pp. 207–219, 1989.

[21] S. Grivet-Talocia, "Enforcing passivity of macromodels via spectral perturbation of Hamiltonian matrices," in *7th IEEE Workshop Signal Propagation Interconnects*, Siena, Italy, May 11–14, 2003, pp. 33–36.

[22] D. Saraswat, R. Achar, and M. Nakhla, "Enforcing passivity for rational function based macromodels of tabulated data," in *12th IEEE Topical Meeting Electrical Performance Electronic Packag.*, Princeton, NJ, Oct. 27–29, 2003, pp. 295–298.

[23] D. Saraswat, R. Achar, and M. Nakhla, "A fast algorithm and practical considerations for passive macromodeling of measured/simulated data," *IEEE Trans. Compon., Packag. Manuf. Technol.*, vol. 27, no. 1, pp. 57–70, Feb. 2004.

[24] D. Saraswat, R. Achar, and M. Nakhla, "Global passivity enforcement algorithm for macromodels of interconnect subnetworks characterized by tabulated data," *IEEE Trans. Very Large ScaIe (VLSI) Syst.*, vol. 13, no. 7, pp. 819–832, Jul. 2005.

[25] S. Grivet-Talocia, "Passivity enforcement via perturbation of Hamiltonian matrices," *IEEE Trans. CAS-I*, vol. 51, no. 9, pp. 1755–1769, Sep. 2004.

[26] S. Grivet-Talocia and A. Ubolli, "On the generation of large passive macromodels for complex interconnect structures," *IEEE Trans. Adv. Packag.*, vol. 29, no. 1, pp. 39–54, Feb. 2006.

[27] S. Grivet-Talocia, "Improving the efficiency of passivity compensation schemes via adaptive sampling," in *14th IEEE Topical Meeting Electrical Performance Electronic Packag.*, Austin, TX, Oct. 24–26, 2005, pp. 231–234.

[28] S. Grivet-Talocia and M. Bandinu, "Improving the convergence of vector fitting in presence of noise," *IEEE Trans. Electromagnetic Compatibility*, vol. 48, no. 1, pp. 104–120, Feb. 2006.

[29] T. Kailath, *Linear Systems*. Englewood Cliffs, NJ: Prentice Hall, 1980.

[30] W. E. Arnoldi, "The principle of minimized iterations in the solution of the matrix eigenvalue problem," *Quart. Appl. Math.*, vol. 9, pp. 17–29, 1951.

[31] Z. Bai, J. Demmel, J. Dongarra, A. Ruhe, and H. van der Vorst, Eds., *Templates for the Solution of Algebraic Eigenvalue Problems: A Practical Guide*. Philadelphia, PA: SIAM, 2000.
[32] E. Chiprout and M. S. Nakhla, "Analysis of interconnects networks using Complex Frequency Hopping (CFH)," *IEEE Trans. Computer-Aided Design*, vol. 14, no. 2, pp. 186–200, Feb. 1995.
[33] J. H. Wilkinson, *The Algebraic Eigenvalue Problem*. London, U.K.: Oxford Univ. Press, 1965.
[34] R. W. Brockett, *Finite Dimensional Linear Systems*. New York: Wiley, 1970.
[35] S. Grivet-Talocia, "Fast passivity enforcement for large and sparse macromodels," in *13th IEEE Topical Meeting Electrical Performance Electronic Packag.*, Portland, OR, Oct. 25–27, 2004, pp. 247–250.
[36] R. Achar and M. Nakhla, "Minimum realization of reduced-order high-speed interconnect macromodels," in *Signal Propagation on Interconnects*, H. Grabinski and P. Nordholz, Eds. Norwell, MA: Kluwer, 1998.
[37] R. Achar, P. K. Gunupudi, M. Nakhla, and E. Chiprout, "Passive interconnect reduction algorithm for distributed/measured networks," *IEEE Trans. Circuits Syst. II: Analog Digit. Signal Process.*, vol. 47, no. 4, pp. 287–301, Apr. 2000.
[38] G. H. Golub and C. F. van Loan, *Matrix Computations*, 3rd ed. Baltimore, MD: Johns Hopkins Univ. Press, 1996.
[39] Y. Saad, *Numerical Methods for Large Eigenvalue Problems*. New York: Halsted Press, 1992.
[40] Y. Saad, "Variations on Arnoldi's method for computing eigenelements of large unsymmetric matrices," *Linear Algebra Its Appl.*, vol. 34, pp. 269–295, 1980.
[41] Matlab Release 14 [Online]. Available: www.mathworks.com
[42] V. Mehrmann and D. Watkins, "Structure-preserving methods for computing eigenpairs of large sparse Skew-Hamiltonian/Hamiltonian pencils," *SIAM J. Sci. Comput.*, vol. 22, no. 6, pp. 1905–1925, 2001.
[43] IdEM 2.4 [Online]. Available: www.emc.polito.it

Stefano Grivet-Talocia (M'98–SM'07) received the Laurea and the Ph.D. degrees in electronic engineering from the Politechnic University of Turin, Turin, Italy.

From 1994 to 1996, he was with the NASA/Goddard Space Flight Center, Greenbelt, MD, where he worked on applications of fractal geometry and wavelet transform to the analysis and processing of geophysical time series. Currently, he is an Associate Professor of Circuit Theory with the Department of Electronics, the Polytechnic of Turin. His current research interests are in passive macromodeling of lumped and distributed interconnect structures, modeling and simulation of fields, circuits, and their interaction, wavelets, time-frequency transforms, and their applications. He is author of more than 80 journal and conference papers.

Dr. Grivet-Talocia served as Associate Editor for the IEEE TRANSACTIONS ON ELECTROMAGNETIC COMPATIBILITY from 1999 to 2001.